

FILE COPY

4

AD-A229 706

Technical Report 1369
October 1990

Systolic Signal Processor/ High Frequency Direction Finding

Final Test Report

J. P. Loughlin
F. M. Tirpak, Jr.

DTIC
ELECTE
DEC 19 1990
S B D
Co

NAVAL OCEAN SYSTEMS CENTER

San Diego, California 92152-5000

J. D. FONTANA, CAPT, USN
Commander

R. M. HILLYER
Technical Director

ADMINISTRATIVE INFORMATION

The study (testing) covered in this report was conducted from October 1989 to October 1990. It was funded by the Naval Sea Systems Command, Washington, DC 20362. The project no. is 76-EE34 01, agency accession no. DN308022, and program element NIF, 604507N. The work was performed by Code 761 of the Naval Ocean Systems Center (NOSC), San Diego, California 92152-5000.

Released by
Dr. G. W. Byram, Head
Processing Research and
Development Branch

Under authority of
K. D. Regan, Head
Space Systems and
Technology Division

ACKNOWLEDGMENTS

The High Speed Systolic Array Processor (HiSSAP) project encompasses work performed over a 7-year period at NOSC. The goal of this project was to obtain a clearer understanding of the complex interactions between parallel processing architecture and adaptive matrix-based signal processing algorithms. Sponsorship of system hardware and software development was initially obtained from the Lasers and Microelectronics NOSC program block managed by Dr. Isaac Lagnado, Code 553. During the intermediate phase of the project, mapping of the multiple signal classification (MUSIC) algorithm and the finite impulse response (FIR) filter onto the testbed hardware was supported by joint sponsorship of the block and major bid and proposal discretionary funding (coordinated by Dr. John Silva, NOSC Office of Technology Research). Integration of these system software applications and the balance of the signal processing/data acquisition components constituted the final phase of the project. Funding for this system integration and the demonstration of the high frequency direction finding application was obtained from the NAVSEA standard matrix processor project (PMS-412), with additional funds supplied by the Lasers and Microelectronics block.

RBT

SUMMARY

OBJECTIVE

This report documents the feasibility of hosting computationally intensive signal processing algorithms on a systolic array architecture. The practicality of such hosting is demonstrated through use of the High Speed Systolic Array Processor (HiSSAP) testbed and a high frequency direction finding algorithm.

RESULTS

Systolic architectures provide a viable alternative to using traditional computer hosts for signal processing applications requiring massive quantities of matrix-based computational throughput. The systolic implementations of a four-channel finite impulse response (FIR) filter and multiple signal classification (MUSIC) direction of arrival estimator yielded results consistent with theoretical models.

RECOMMENDATIONS

The tests conducted on the HiSSAP testbed demonstrated the feasibility of experimental data produced by both an analytical model and an antenna simulator within a controlled laboratory signal environment. The scope of this investigation should be expanded to include processing of actual off-the-air high frequency radio signals. This advanced level of testing can more realistically estimate the essential design specifications for a proper systolic host for adaptive signal processing algorithms. (KR)

Accession For	
NTIS GRA&I	<input checked="" type="checkbox"/>
DTIC TAB	<input type="checkbox"/>
Unannounced	<input type="checkbox"/>
Justification	
By _____	
Distribution/	
Availability Codes	
Dist	Avail and/or Special
A-1	



CONTENTS

INTRODUCTION	1
SCOPE	1
METHODOLOGY	1
DESIGN APPROACH	2
TESTING APPROACH	2
TEST RESULTS	3
Analytical Data Testing	3
Experimental Data Testing	5
REFERENCE	8
APPENDIX A: SIMULATOR IMPLEMENTATION	A-1
ANTENNA SIMULATOR	A-2
APPENDIX B: INTEGRATION TESTS	B-1
DATA ACQUISITION SUBSYSTEM	B-2
Signal to Noise	B-2
Linearity	B-2
FINITE IMPULSE RESPONSE FILTER	B-3
Frequency Response	B-3
Phase Quadrature Data Construction	B-6

FIGURES

1a. Spatial output spectrum, contour plot, analytical full scale input data, PC host. . . .	3
1b. Spatial output spectrum, mesh plot, analytical full scale input data, PC host.	3
2a. Spatial output spectrum, contour plot, analytical attenuated input data, PC host. . .	4
2b. Spatial output spectrum, mesh plot, analytical attenuated input data, PC host. . . .	4
3. Direction finding experiment, block diagram.	5
4a. Spatial output spectrum, contour plot, experimental input data, PC host.	6
4b. Spatial output spectrum, mesh plot, experimental input data, PC host.	6
5. Spatial output spectrum, mesh plot, experimental input data, HiSSAP host.	6
6a. Spatial output spectrum, contour plot, experimental input data, PC host.	7
6b. Spatial output spectrum, mesh plot, experimental and attenuated input data, PC host.	7
7a. Spatial output spectrum, contour plot, recalibrated experimental input data, HiSSAP host.	8

7b. Spatial output spectrum, mesh plot, recalibrated experimental input data, HiSSAP host.	8
A-1. Wavefront simulator functional block diagram.	A-2
A-2. Azimuthal profile of antenna/signal model.	A-3
A-3. Elevation profile of antenna/signal model.	A-3
A-4. Angular definitions of antenna/signal model.	A-4
B-1. Data acquisition—broadband output spectrum.	B-2
B-2. Narrowband filter output spectrum, two-tone input.	B-3
B-3. Narrowband filter output spectrum, single-tone input.	B-5
B-4. Narrowband filter output spectrum, composite multitone input.	B-6
B-5. Narrowband filter output spectrum, linear time epoch of sampled data.	B-7
B-6. Narrowband filter output spectrum, complex mapping of sample data.	B-7

TABLES

1. Test signal specifications.	4
2. Antenna placement.	4
3. Test signal specifications.	7
4. Antenna placement.	7
A-1. Wavefront simulator delays, 0° elevation.	A-5
A-2. Wavefront simulator delays, 10° elevation.	A-5
B-1. FIR filter design specifications.	B-4

INTRODUCTION

The Naval Ocean Systems Center (NOSC) is investigating the integration of high speed array processing architectures and advanced matrix-based signal processing algorithms. The purpose of the High Speed Systolic Array Processor (HiSSAP) testbed project is to demonstrate the feasibility of hosting computationally intensive signal processing algorithms on a systolic array architecture.

The first application selected for mapping onto the HiSSAP processor was a high frequency (HF) direction of arrival estimator. To realize a system implementation of such an application, the multiple signal classification (MUSIC) algorithm was mated to a bank of finite impulse response (FIR) filters and a four-channel data acquisition subsystem. A complete description of the systolic mapping of the MUSIC algorithm and FIR filters is available elsewhere* and also in reference 1; only brief references to this mapping activity will be presented here.

SCOPE

The tests performed are intended to demonstrate the mapping feasibility of this direction finding application on a systolic architecture and are not intended to address the complex signal environment normally encountered in the high frequency radio band. For this reason, several design assumptions and testing constraints have been adopted to maintain the intended focus of the demonstration. The generalized structure of the MUSIC algorithm is capable of simultaneously localizing the directions of arrival (DOA) of multiple signal sources. Initial implementation of the MUSIC algorithm on the HiSSAP testbed hardware enabled processing data obtained from a sensor array of four elements. Operating with an array of this dimension allowed the MUSIC algorithm to resolve the presence and DOA of no more than three simultaneous signals. In the HF environment, more signals (many more in some cases) will most likely be present in any given communications channel. With the laboratory testing fixture used, such an overabundance of signals was avoided. An additional constraint was placed on the structure of the input data to maximize the computational efficiency in mapping the MUSIC algorithm on the systolic array. A maximum of two simultaneous input signals was chosen as a practical signal model for the tests performed.

METHODOLOGY

Samples of the sensor array output are produced by the data acquisition subsystem. The 10-megasample conversion rate, and the 12-bit output resolution, limit the allowable band of frequencies and signal levels that can be used for system testing. The signals used for the tests described were confined to the low HF band (2.5 through 4.5 MHz). Also, the signal levels were carefully adjusted to maximize the dynamic range of the A/D conversion processes.

Sinusoidal signals without any form of modulation were used throughout the system tests. Normally, this modulation provides the decorrelation needed to enable the MUSIC algorithm to discriminate the presence of multiple signals. To satisfy this requirement, the frequency of each signal was offset from the selected channel center frequency. The magnitude of this offset was chosen to ensure uncorrelated test signals over the interval in which the DOA estimate was computed.

Great care was taken in specifying the sensor array and signal spatial parameters, due to the high spatial resolution achievable using an advanced algorithm such as MUSIC. It was difficult and time-consuming to accurately translate the signal model from the software simulation program to its laboratory hardware equivalent. Therefore, a limited number of test scenarios were performed, once comparable results were obtained with the development algorithm models and the systolic implementation.

*Working paper, titled, Design and Implementation of a Multistage Narrowband FIR Filter on the High-Speed Systolic Array Processor (HiSSAP), by F. M. Tirpak of NOSC for NAVSEA PMS-412, September 1, 1989.

DESIGN APPROACH

During the initial development of the HiSSAP direction of arrival estimator, the MUSIC algorithm and FIR filters were modeled on a personal computer (PC). MATLAB provided the analytical environment to formulate and test mapping implementations prior to systolic programming efforts.

A detailed description of the FIR filter development is contained in a separate engineering technical publication (refer to footnoted working paper). Development of the MUSIC algorithm on the PC was undertaken in two separate phases, sequential and parallel realizations. Under the sequential phase, matrix operations, such as the QR decomposition and the singular value decomposition (SVD), contained within MATLAB as standard library calls, were utilized to validate the baseline operation of the MUSIC algorithm. In the next phase of the development, these intrinsically parallel operations were custom-mapped across multiple processes in MATLAB. Using this advanced model, issues were resolved concerning data movement, computational requirements, and array partitioning within a systolic architecture.

Mapping the MUSIC algorithm onto the HiSSAP testbed involved translating the software modules defined during the parallel modeling phase just described. The diagnostic resources of the HiSSAP testbed provided a method for testing the systolic implementation of MUSIC with simulated data identical to that used for the sequential and parallel implementations on the PC. Additional software modules were written to support interfacing the FIR filter and the input steering vectors to the MUSIC algorithm.

TESTING APPROACH

Initial testing of the MUSIC algorithm involved processing data created by the antenna simulation program executing on the personal computer. This test program was written to translate user descriptions of antenna and signal geometries into simulated antenna array output and steering vector data. A description of this model and details of its software implementation are presented in Appendix A of this report. A signal model utilizing a planar array of four omnidirectional antennas and two signal sources was used for all of the tests performed. The diameter of the array was chosen to ensure useful spatial apertures under the test conditions. Antenna simulator output, referred to as the "analytical data," was applied to both PC-based simulation models of MUSIC, as well as to the systolic implementation. These spatial response outputs were carefully compared to verify that computational equivalence was maintained.

Once functional equivalence was established, subsequent testing of the algorithm involved processing input from the antenna wavefront simulator. This input is referred to as the "experimental data." The tests were confined to the lower HF frequency band due to the maximum sampling rate (10-M samples/s) used in the data acquisition subsystem.

This four-channel hardware antenna simulator, using laboratory signal sources, was constructed to replace the analytical antenna simulator program. Through a system of power splitters/summers and analog tapped lumped-parameter delay lines, signals with selected angles of arrival could be constructed and applied to the data acquisition subsystem of the testbed.

Using the diagnostic ports of the testbed hardware, data samples (identified for processing by the testbed MUSIC software) were intercepted and transferred to the PC for analysis. Using the sequential and parallel MUSIC models residing on the PC development host, a baseline spatial response output was generated. This procedure was also needed to verify proper calibration of the antenna simulator.

Finally, the integrated operation of the systolic FIR filter and MUSIC algorithm was compared with the baseline response obtained from the software models.

TEST RESULTS

The output of the MUSIC algorithm is a response-magnitude matrix with ordinates of azimuth and elevation. A separate matrix of input steering vectors is used to identify the complete set of possible arrival directions resolvable by MUSIC. This collection of steering vectors customarily spans, in uniform increments, the azimuth and elevation space of interest. During development of the sequential and parallel models of the MUSIC algorithm, an array of 1980 steering vectors was used. Arrival angles of -22 through $+22$ degrees azimuth and 0 through 43 degrees elevation (in increments of 1 degree) were represented by the matrix of steering vectors.

While testing MUSIC on the systolic testbed, these complex vectors were loaded into the systolic hardware before initiating the MUSIC algorithm. Due to memory limitations existing on the systolic input/output modules, the number of elements contained within the steering vector matrix was reduced to half (0 through 21 degrees elevation). This down-sizing of the steering vector matrix does not affect the quality of the spatial estimation produced but does change the scaling of the graphical output. For comparison, a down-sized steering vector matrix was used for both the software (sequential and parallel) models and the systolic testbed implementation during the final phases of system testing. Two graphical output formats were used to display the response of the three implementations of the MUSIC algorithm. The 3-D mesh format facilitates visualizing response peaks, while the 2-D contour format helps to accurately localize arrival angles.

Analytical Data Testing

Figures 1a and b show the baseline response of the sequential model of MUSIC to the analytical data matrix input constructed using the parameters in tables 1 and 2. These plots clearly indicate the presence of two signals with the directions of arrival correctly identified by the well-defined response peaks. The parallel model of MUSIC produced an identical response. After transferring this simulated input data from the PC to the testbed hardware, the systolic implementation of the MUSIC algorithm produced an essentially identical response.

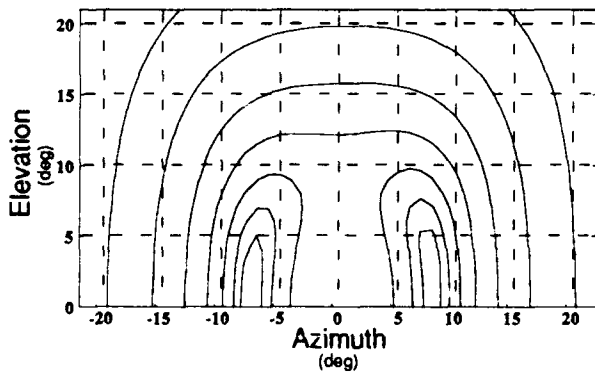


Figure 1a. Spatial output spectrum, contour plot, analytical full scale input data, PC host.

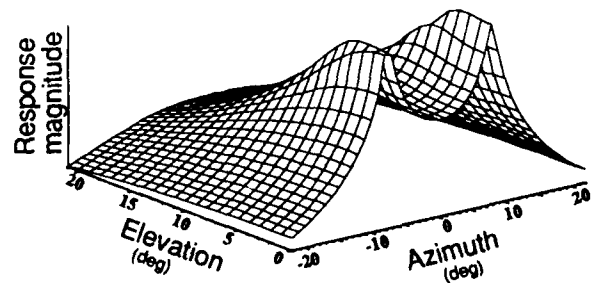


Figure 1b. Spatial output spectrum, mesh plot, analytical full scale input data, PC host.

Table 1. Test signal specifications.

Source	Frequency (MHz)	Amplitude (dB)	Azimuth (deg)	Elevation (deg)
Signal 1	2.751000	0 dB	+6.61	0
Signal 2	2.751500	0 dB	-6.61	0

Table 2. Antenna placement.

Antenna	X Position (% wavelength)	Y Position (% wavelength)
1	120	0
2	0	120
3	-120	0
4	0	-120

The performance of the algorithm was then tested under noisy signal conditions. Another set of analytical data was constructed using parameters similar to those in table 1, except for applying uncorrelated gaussian noise to each channel at the -3-dB level. Figures 2a and b show the response of the sequential MUSIC model, typifying that of the parallel model. The predictable effect of noise in the input data is a softening of both response peaks. A more subtle effect is a bias factor that displaces the location of these peaks. This phenomenon may result from a natural tendency of MUSIC to produce response biases when processing ill-conditioned input data and should be further studied. This analytical data was then transferred to the systolic testbed and processed to yield a response exhibiting identical characteristics.

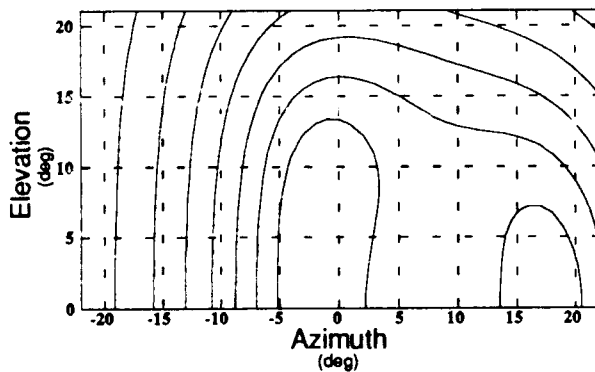


Figure 2a. Spatial output spectrum, contour plot, analytical attenuated input data, PC host.

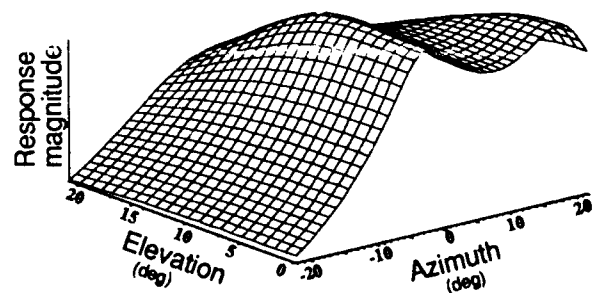


Figure 2b. Spatial output spectrum, mesh plot, analytical attenuated input data, PC host.

Once the functional integrity of the MUSIC algorithm hosted on the systolic testbed was demonstrated for analytical data, we began integrating the remaining components of the signal processing system. A series of tests was performed on the data acquisition/FIR filter components of the signal processor. The results of these tests are documented in Appendix B, Integration Tests.

Figure 3 is a block diagram depicting the addition of the data acquisition subsystem and the systolic FIR filter. The analytical signal generator was replaced with laboratory oscillators and the hardware wavefront simulator. Appendix A describes implementation of the simulator and the mathematical equations that govern the test configuration of this hardware. Once digitized by the data acquisition subsystem, the FIR filter on the systolic hardware filtered and down converted the sinusoidal test signals from the wavefront simulator to baseband complex samples. Spatial responses (comparable to those previously described in the "analytical data testing" section) were generated by this test fixture.

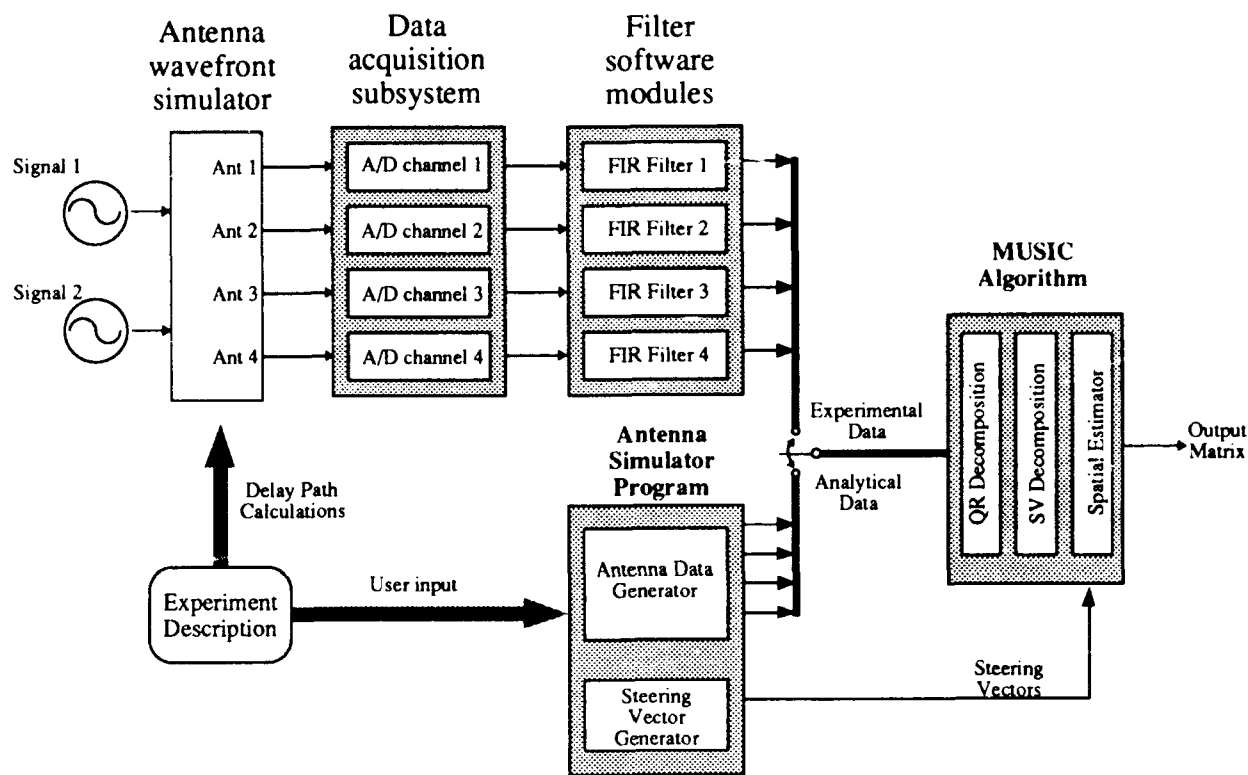


Figure 3. Direction finding experiment, block diagram.

Experimental Data Testing

The wavefront simulator was configured to duplicate the test conditions previously used (tables 1 and 2). Figures 4a and b show the response of the sequential model to the data input from the hardware wavefront simulator. These spatial response plots show the combined impact of calibration errors in the antenna wavefront simulator and the signal quantization within the data acquisition subsystem. The apparent softening of the response peak and accompanying position bias indicate the likelihood that this setting of the wavefront simulator produced ill-conditioned data.

In subsequent testing, these sampled data were processed by the systolic MUSIC algorithm. Figure 5 shows the spatial response obtained from the testbed hardware under the same signal conditions. This illustration clearly demonstrates that the input data produced under these test conditions stressed the computational precision of the systolic processor beyond its limits. Further investigation revealed that numerical underflow faults in several systolic elements were caused by ill-conditioned input data.

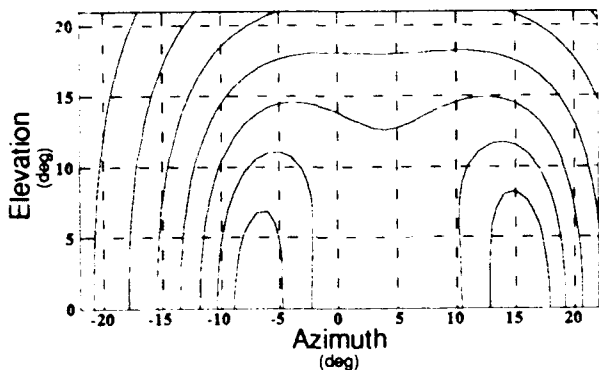


Figure 4a. Spatial output spectrum, contour plot, experimental input data, PC host.

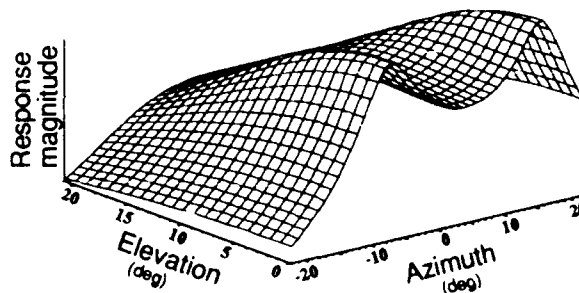


Figure 4b. Spatial output spectrum, mesh plot, experimental input data, PC host.

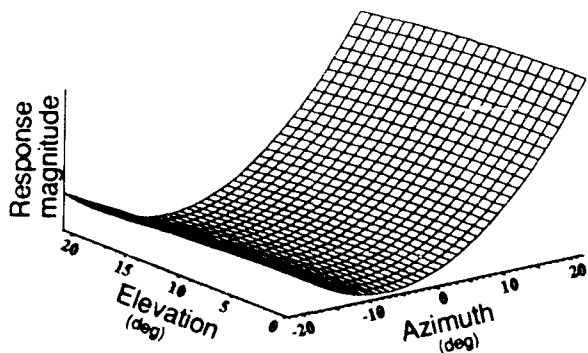


Figure 5. Spatial output spectrum, mesh plot, experimental input data, HiSSAP host.

Note the different computational stability observed between the developmental models and the systolic implementation. Computations are performed to double (64 bit) precision in the PC MATLAB algorithm models hosted on the personal computer, compared with the single word precision used in the systolic array testbed hardware. As the vertical arrival angle approaches 0 degree (groundwave), the effective aperture of the antenna array in that dimension diminishes to 0. This condition leads to column dependencies of the data input to the MUSIC algorithm. The degree to which the algorithm can successfully operate with ill-conditioned data is greatly influenced by the numerical precision used.

Another test was performed in an attempt to isolate the cause of the numerical underflow. The magnitude of the test signals was reduced 3 dB below the full-scale setting used initially. Adjusting the test signal level in the presence of the quantization noise of the A/D converters was equivalent to reducing the signal to noise (SNR) by 3 dB. The effect of this additional uncorrelated noise was to increase the computational stress on the MUSIC algorithm. The output of the MATLAB model of MUSIC (figures 6a and b) shows both a complete merging of the response peaks and a strong bias of the estimate of arrival angle. Systolic implementation of the algorithm continued to suffer from underflow errors and again was not able to generate a useful spatial estimate.

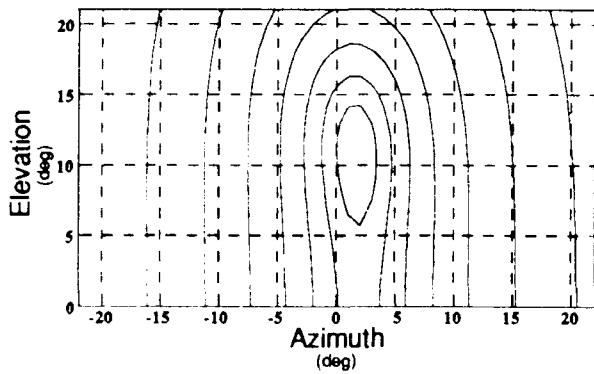


Figure 6a. Spatial output spectrum, contour plot, experimental input data, PC host.

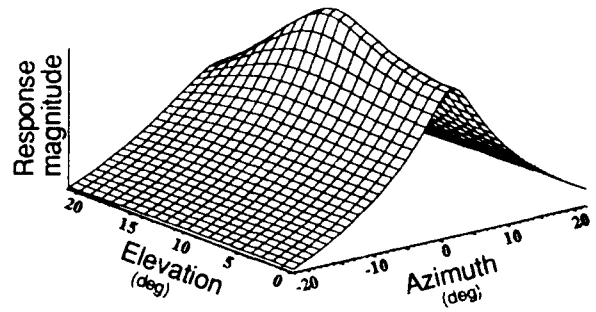


Figure 6b. Spatial output spectrum, mesh plot, experimental and attenuated input data, PC host.

A new test scenario was adopted that was predicted to produce input data exhibiting a much lower condition number. The diameter of the antenna array was enlarged relative to the wavelength of the test signals used. In addition, an elevation angle of 10 degrees was selected to increase the vertical aperture. Both of these changes reduce the numerical precision required to perform the computations contained within the MUSIC algorithm. The wavefront simulator was recalibrated, and a new matrix of steering vectors was constructed to reflect the testing scenario specified in tables 3 and 4.

Table 3. Test signal specifications.

Source	Frequency (MHz)	Amplitude (dB)	Azimuth (deg)	Elevation (deg)
Signal 1	2.751000	0 dB	+6.42	10
Signal 2	2.751500	0 dB	-8.00	10

Table 4. Antenna placement.

Antenna	X Position (% wavelength)	Y Position (% wavelength)
1	315	0
2	0	315
3	-315	0
4	0	-315

Figures 7a and b show the spatial response of the systolic MUSIC under the new test conditions. Identical responses were also obtained from the sequential and parallel models on MATLAB.

The factor of antenna aperture is particularly apparent in this response. The sharpness of the response in the azimuthal dimension demonstrates the large effective horizontal aperture realized by the antenna array. Since its azimuthal direction of arrival straddles two resolution bins, the magnitude of the response peak associated with signal 1 (arriving at 6.42 degrees) is somewhat diminished. The response to signal 2 (arriving at -8.00 degrees) is sharp and demonstrates the resolution achievable with the systolic implementation of the MUSIC algorithm. Apparent resolution in the elevation dimension is significantly poorer

due to the limited vertical aperture existing for this test geometry. Note that the apparent resolution achieved by implementing the MUSIC algorithm is profoundly influenced by interactions of several system design factors. In addition to sensor array aperture, the structure of the steering vectors and numerical precision of the computations are also coupled to the ultimate spatial resolution achievable with MUSIC.

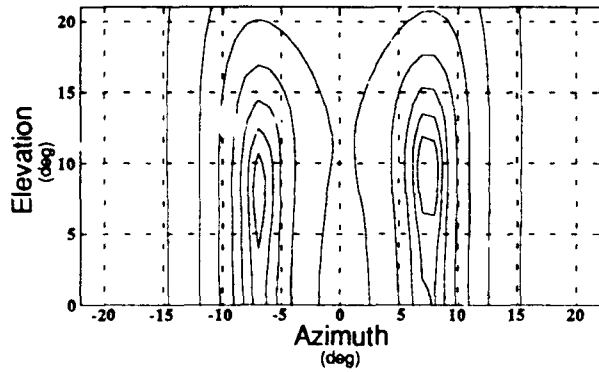


Figure 7a. Spatial output spectrum, contour plot, recalibrated experimental input data, HiSSAP host.

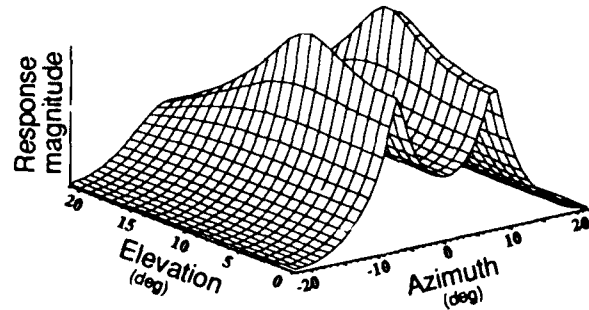


Figure 7b. Spatial output spectrum, mesh plot, recalibrated experimental input data, HiSSAP host.

REFERENCE

1. J. P. Loughlin. 1988. "Multiple Signal Classification (MUSIC) Algorithm Hosted on the High Speed Systolic Array Processor (HiSSAP)," *SPIE Proceedings*, vol. 977, August 1988.

APPENDIX A
SIMULATOR IMPLEMENTATION

APPENDIX A

SIMULATOR IMPLEMENTATION

ANTENNA SIMULATOR

Testing in the second phase of the high frequency direction finding experiment was conducted using a bench-top antenna simulator operating in the lower portion of the high frequency band (2 through 4.5 MHz). Each output of two sinusoidal signal generators was passed through a delay network via a power splitter.

The transit time for a propagating flat wavefront to impinge on each element in an antenna array is represented by a separate delayed signal path in the wavefront simulator. Corresponding pairs of delay paths associated with each test signal are summed to form each antenna output signal (figure A-1). Each delay path within the wavefront simulator is realized in one of two ways: (1) utilizing one of multiple taps available from a lumped parameter dual inline package (DIP) transmission line unit, or (2) utilizing one such delay tap combined with a section of coaxial cable. Ten equally spaced taps on the transmission line may provide up to 1000 nanoseconds of delay for each signal source. Trimming of coaxial cable enables construction of arbitrary delays within the measurement accuracy of the laboratory setup (5 nanoseconds).

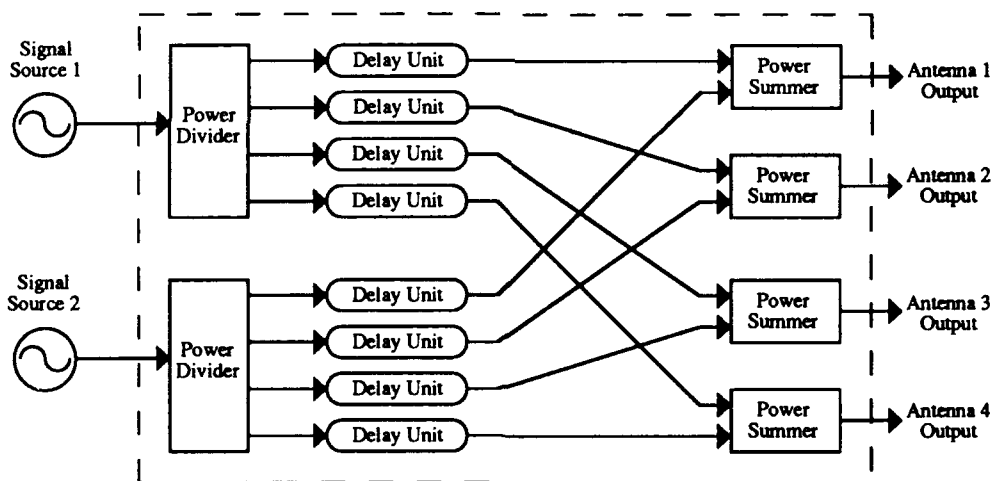


Figure A-1. Wavefront simulator functional block diagram.

This wavefront simulator provides four analog signals to the data acquisition subsystem of the systolic testbed via equal length coaxial cables. These signals represent the outputs from four idealized omnidirectional antennas placed on a ground plane at locations equidistant about the circumference of an imaginary circle (figure A-2). The diameter of this circle is chosen to yield useful array apertures for the wavelength of the signals to be received (approximately 2.75 MHz). For the tests conducted, a diameter ranging from 2 to 6 wavelengths was used. The horizontal aperture of the array is defined as the linear dimension (expressed in wavelengths) that a horizontal projection of the antenna array forms on a plane parallel to the approaching wavefront.

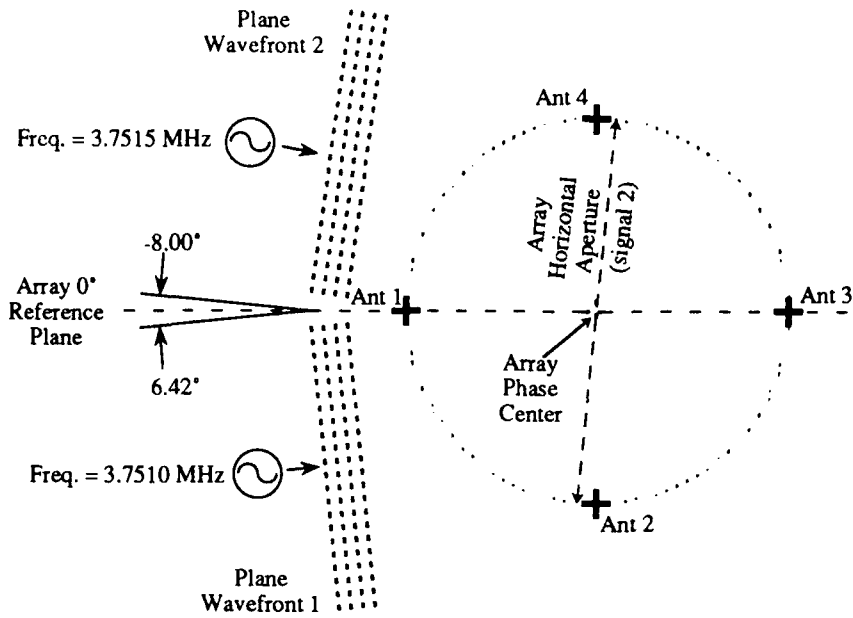


Figure A-2. Azimuthal profile of antenna/signal model.

Azimuthal angles are measured with respect to the reference plane of symmetry. Actual arrival angles chosen for the tests were based on convenient delay taps existing in the antenna wavefront simulator hardware. The antenna array is assumed to be placed on a nonreflecting ground plane, and the height of each antenna element is negligible compared to the array's overall dimension (figure A-3). These assumptions enable the ground plane to serve as the reference for measuring arrival angle elevation.

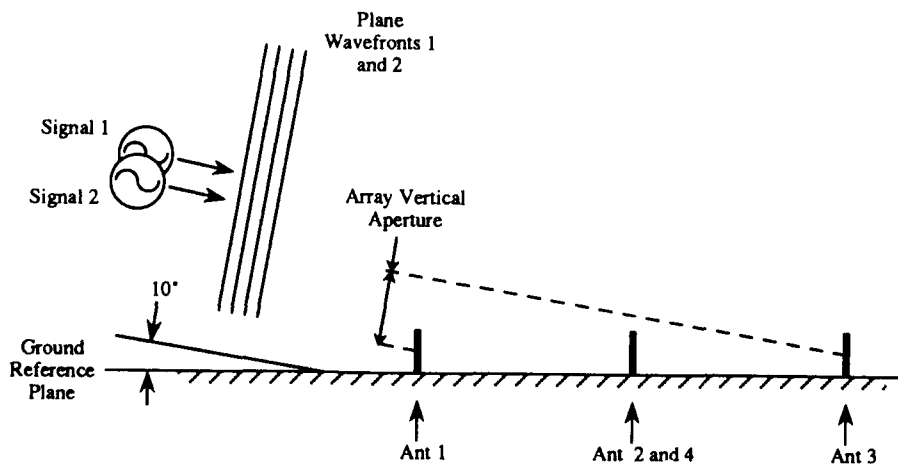


Figure A-3. Elevation profile of antenna/signal model.

Experimental data were generated using either an elevation angle specification of 0 or 10 degrees. Selection of identical elevation angles for both signal sources was merely for the convenience of simulation and was not due to any limitation in the operation of the MUSIC algorithm.

The vertical aperture of the array is defined as the linear dimension (expressed in signal wavelengths) that a vertical projection of the antenna array forms on a plane parallel to the approaching wavefront.

Calculation of the delay values used in the wavefront simulator is based on the antenna diagram (figure A-4). Signal arrival angle is decomposed into the relative azimuthal bearing (expressed as ϕ) and an elevation bearing ($90^\circ - \theta$). Azimuthal angle of arrival is defined relative to the axis of symmetry that passes through antennas 1 and 3. For the tests conducted, the azimuthal components of the two arrival angles were restricted to values no greater than ± 22 degrees off the plane of antenna array symmetry (the x axis). This constraint dictates that both signal wavefronts first impinge the sensor array at antenna 1. The following equations express the propagation delay relative to antenna 1.

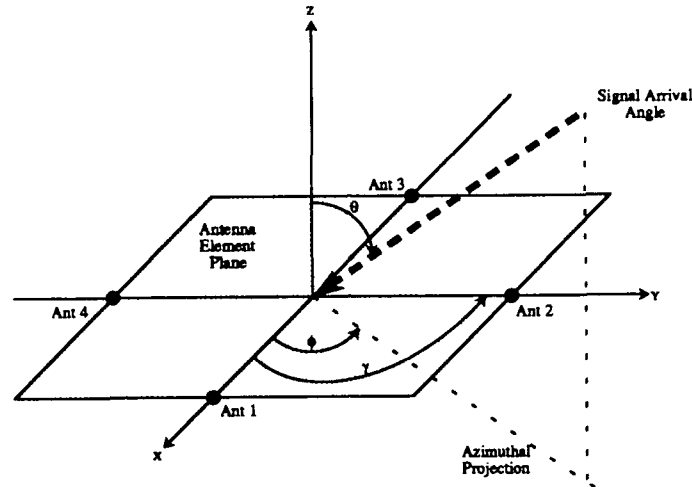


Figure A-4. Angular definitions of antenna/signal model.

The geometric center of the antenna array is typically assumed to be the datum reference point for calculating delays. However, antenna 1 was used as the datum reference point, allowing a reduction in the complexity of the wavefront simulator. The first delay device was reduced to a trivial feedthrough (zero delay) path. Further simplicity was attained by assigning an existing fixed tap delay to antenna 2 for signal source 1. A comparable and symmetric tap delay was used for antenna 3 and signal source 2. Once the exact delays of these taps were measured, an equivalent azimuthal arrival direction was calculated using equation (3) as follows:

$$\begin{aligned}
 \tau_1 - \tau_2 &= \tau_r \cos(\gamma_1 - \phi) \sin(\theta) - \tau_r \cos(\gamma_2 - \phi) \sin(\theta) & (1) \\
 &= \tau_r \sin(\theta) [\cos(\gamma_1 - \phi) - \cos(\gamma_2 - \phi)] \\
 &= \tau_r \sin(\theta) \left\{ -2 \sin \left[\frac{1}{2} (\gamma_1 - \phi - \gamma_2 + \phi) \right] \sin \left[\frac{1}{2} (\gamma_1 - \phi + \gamma_2 - \phi) \right] \right\} \\
 &= -2\tau_r \sin(\theta) \left[\sin \frac{1}{2} (\gamma_1 - \gamma_2) \sin \frac{1}{2} (\gamma_1 + \gamma_2 - 2\phi) \right], \\
 &\left(\text{note } \gamma_1 = 0, \gamma_2 = \frac{\pi}{2}, \rightarrow \sin \frac{1}{2} (\gamma_1 - \gamma_2) = -\frac{1}{\sqrt{2}} \right)
 \end{aligned}$$

$$\rightarrow \tau_1 - \tau_2 = \sqrt{2} \tau_r \sin\left(\frac{\gamma_2}{2} - \phi\right) \sin(\theta) \quad (2)$$

or

$$\phi = \frac{\gamma_2}{2} - \sin^{-1}\left[\frac{\tau_1 - \tau_2}{\sqrt{2} \tau_r \sin(\theta)}\right] \quad (3)$$

The delay values for the remaining antenna/signal paths equation (2) established the elevation angles of each experiment. These final four delay paths (two per signal source) were constructed from a combination of existing delay taps and custom-cut coaxial cables.

Each of the signal delay paths (d_n) relative to the center of the antenna array was computed. Using antenna 1 as the datum, the delays were adjusted to yield only positive values. These delays (signified by $\tau_1 - \tau_n$) were assigned to the corresponding signal paths within the antenna wavefront simulator. Tables A-1 and A-2 list the delay values used for the test scenarios described in this report.

Table A-1. Wavefront simulator delays, 0° elevation.

Source	d_1	d_2	d_3	d_4	τ_{1-2}	τ_{1-3}	τ_{1-4}
Signal 1	124.1	14.4	-124.1	-14.4	109.7	248.3	138.5
Signal 2	124.1	-14.4	-124.1	14.4	138.5	248.3	109.7

Table A-2. Wavefront simulator delays, 10° elevation.

Source	d_1	d_2	d_3	d_4	τ_{1-2}	τ_{1-3}	τ_{1-4}
Signal 1	344.5	38.8	-344.5	-38.8	305.7	689	392.4
Signal 2	343.3	-48.2	-343.3	48.2	391.5	686	295.1

APPENDIX B
INTEGRATION TESTS

APPENDIX B

INTEGRATION TESTS

DATA ACQUISITION SUBSYSTEM

Signal to Noise

Proper operation of the data acquisition system was verified by using a single tone FFT test. A 2.50-MHz test sinusoid was sequentially applied to the RF input of each A/D converter board in the system. The board input level was adjusted to be -33 dBm to achieve a full scale signal of 2.50 volts p-p at the input to the internal A/D converter. A data block composed of 4096 digital samples (acquired at a 10-MHz rate) was constructed in each of the four systolic elements within the top row of the testbed processor array. Once collected, these samples were transferred from the top row of arithmetic processing modules (APM) to the PC via the diagnostic port of the HiSSAP system. Using a library utility contained within PC MATLAB, a 4-K FFT analysis of the test data was performed, and the spectral output is depicted in figure B-1. This plot shows the responses obtained for each of the four converter channels. To maintain the maximum spectral resolution, no input data windowing was used. The apparent noise floor deviates from flat due to artifacts associated with creating the FFT. A small amount of frequency error in either the test signal or the data acquisition sampling clock caused samples within the output data block to describe a noninteger number of sinusoidal cycles. Distribution of noise energy is relatively uniform except for spurious response peaks appearing at 0.5 MHz increments across the spectrum. Presence of this energy suggests coupling of the acquisition clock (10 MHz) into the signal path. This residual is quite low and localized to well-defined frequencies and did not interfere with the overall system testing. The measured SNR for this test was 42 dB.

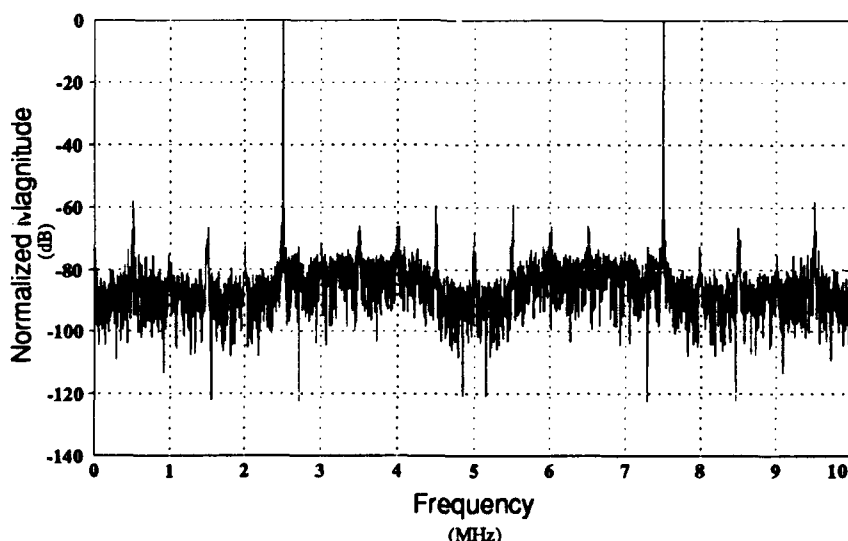


Figure B-1. Data acquisition—broadband output spectrum.

Linearity

A test of the linearity of the A/D converters was conducted using a two-tone test. For this test, two RF sinusoids were applied to the input of each channel of the systolic testbed. Once digitized, the data

samples were passed through the narrowband filter (described in the following section) to enhance the spectral resolution of this intermodulation test. The frequency offset of each signal was selected to ensure that both sinusoids appear in the base-banded output of the filter (in this case, 400 and 2000 Hz above the filter center frequency). The spectrum of the filter's response to these equal amplitude test signals is shown in figure B-2. Intermodulation products ($n \cdot f_1 + m \cdot f_2$) appear to be greater than 30 dB below either test tone. Again, the side-lobe responses of the test tone limited the dynamic range of the test.

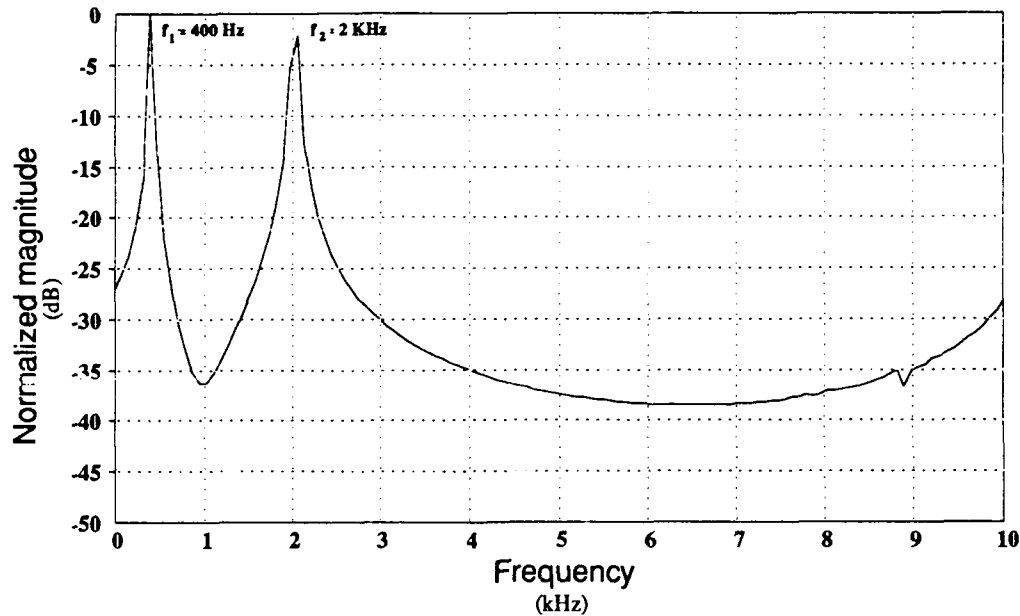


Figure B-2. Narrowband filter output spectrum, two-tone input.

FINITE IMPULSE RESPONSE FILTER

Frequency Response

Table B-1 itemizes the design specifications of the filter mapped onto the systolic testbed. The filters are programmed to process the wideband data outputs of the four A/D converters (BW = 5 MHz) and produce corresponding narrowband complex outputs (BW = 6 kHz) suitable for subsequent processing by the MUSIC algorithm. In addition to producing narrowband signal samples, each FIR filter shifts the center of its output passband to zero frequency through a system of desampling and complex heterodyning. The factor of approximately 1000 to 1 in bandwidth reduction is achieved by cascading three stages of internal filtering. An input block of 170-k samples which have been acquired at a 10-Msample/second rate is reduced to 170 complex output samples. Depending on the coefficients used in the heterodyning operation, the signal energy of any arbitrary RF narrowband channel can be placed in the baseband spectrum of these 170 output samples. To minimize the transient filter response associated with block-processed input data, the initial 42 complex output samples produced by the filter are considered as transient energy and are discarded. The remaining 128 transient-free data samples from each channel are passed to the MUSIC algorithm.

Table B-1. FIR filter design specifications.

Parameter	Symbol	Design Goal	Units
Passband Corner Frequency	f_c	2.2	(kHz)
Stopband Corner Frequency	f_r	3.1	(kHz)
Stopband Rejection		>60	(dB)
Passband Center Frequency	f_c	2.5 - 4.5	(MHz)
Input Data Block Size		170 k	(real samples)
Output Data Block Size		170	(complex samples)
Input Data Rate	$F_{s \text{ in}}$	10 M	samples/second
Output Data Rate	$F_{s \text{ out}}$	10 k	samples/second

Several tests were performed to establish the functionality of the FIR filters hosted on the systolic array. For the integration phase of the mapping effort, the four filter modules hosted on the systolic hardware processed data obtained from the data acquisition subsystem. The tests utilized one or more input signals that were applied to each of the four corresponding A/D converter modules via the antenna wavefront simulator. During the tests, variable amounts of frequency offset were introduced between the test signals and the design center frequency of the filter. This offset allowed meaningful FFT and phase analysis of the filter output samples.

A test RF signal with a frequency offset of 80 Hz from the filter center frequency was input to the data acquisition subsystem and processed by one channel of the filter on the systolic testbed. This initial test served to verify the proper operation of the FIR filter on 12-bit digitized data. At the system sampling frequency and data block size used, this 80-Hz offset resulted in capturing one complete cycle of the test sinusoid at the output of the filter. Figure B-3 shows the output spectrum of the filter.

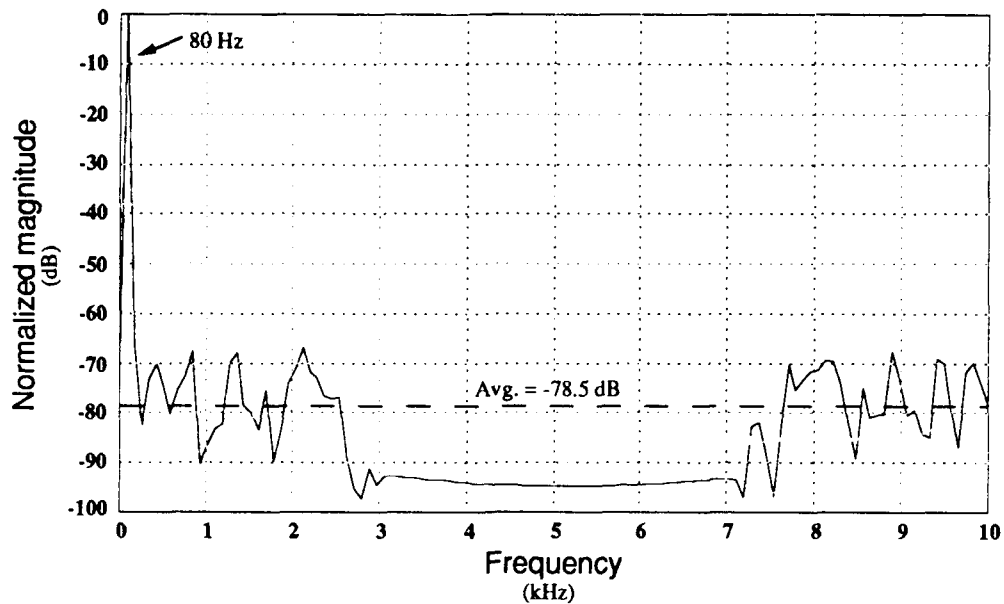


Figure B-3. Narrowband filter output spectrum, single-tone input.

The average noise is the statistical mean of the FFT coefficients over the filter's passband after the test signal has been excised. When expressed as a ratio to the power of the full scale test signal, this measurement yielded -78.5 -dB average noise power energy (as indicated in figure B-3). This measurement closely matches the corresponding metric at the wideband output of the data acquisition subsystem. This comparison demonstrates proper filter operation in which no out-of-band noise energy has been "folded" into the baseband output response. The noise envelope at the output of the filter indicates the baseband frequency response to wideband noise. Although a 2.5 -kHz passband corner frequency can be approximated from the shape of the noise response, the stopband characteristics are obscure in this plot. Residual signal energy appearing in the 3 - to 7 -kHz region of the spectral output is most likely caused by the error in capturing exactly one cycle of baseband signal data in the 128 samples output from the FIR filter. This noninteger relationship between the FFT sample size and the period of the test signal causes the appearance of side-lobe response skirts.

A second test was performed to more accurately measure the baseband frequency response of the filter. Overall frequency response was assessed by merging individual responses to a spectral distribution of individual test tones. The response envelope that summarizes the results of these tests appears in figure B-4. The corner frequency for the passband occurred at 2.2 kHz. The band-reject region (>60 dB down) appeared to begin at 3 kHz, but, due to the side-lobe artifacts present in the output of the FFT, the measurement dynamic range was limited to about 45 dB. The indications were that each of the four filter channels exhibited the performance levels described in the design specifications of table B-1.

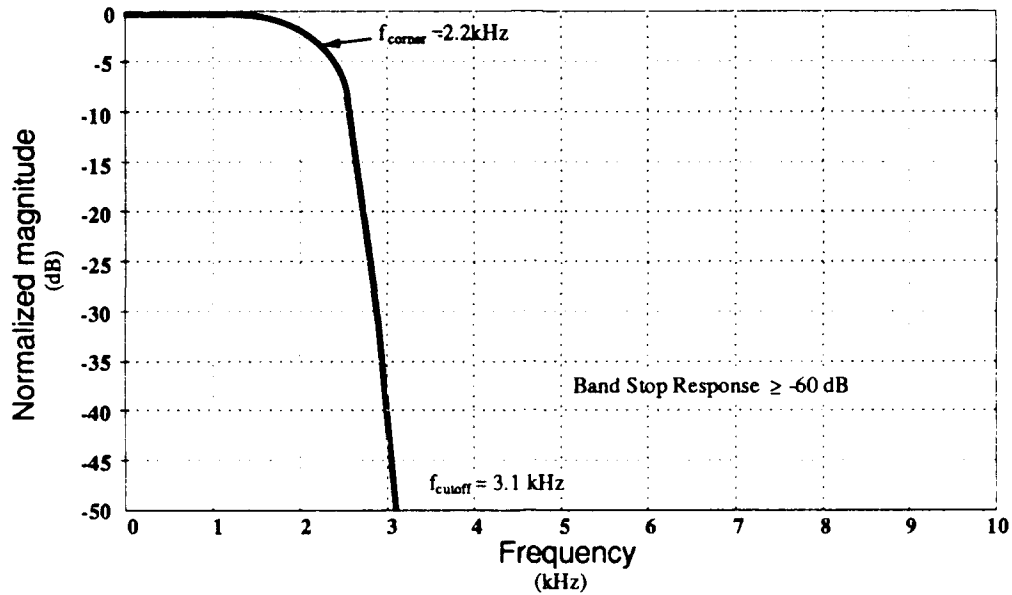


Figure B-4. Narrowband filter output spectrum, composite multitone input.

Phase Quadrature Data Construction

The filter constructs complex baseband samples from real input samples. The direction of arrival estimate generated by the MUSIC algorithm is based solely on the relative phase information contained in the sensor-array output. Errors in constructing the complex samples at the filter output can result in the response biases or the ultimate failure of MUSIC to construct useful DOA spatial spectrums. A test was performed to verify the accuracy of the complex samples constructed by the filter. Using RF test signals of various frequency offsets, this characteristic of the filter was studied. The output of one such test (figure B-5) shows the superposition of in-phase and quadrature samples of a 100-Hz sinusoidal output waveform. Matched amplitude and 90-degree phase shift between the two signal components indicate proper filter operation. An alternate display format plotting real versus imaginary output samples produces a circle (figure B-6).

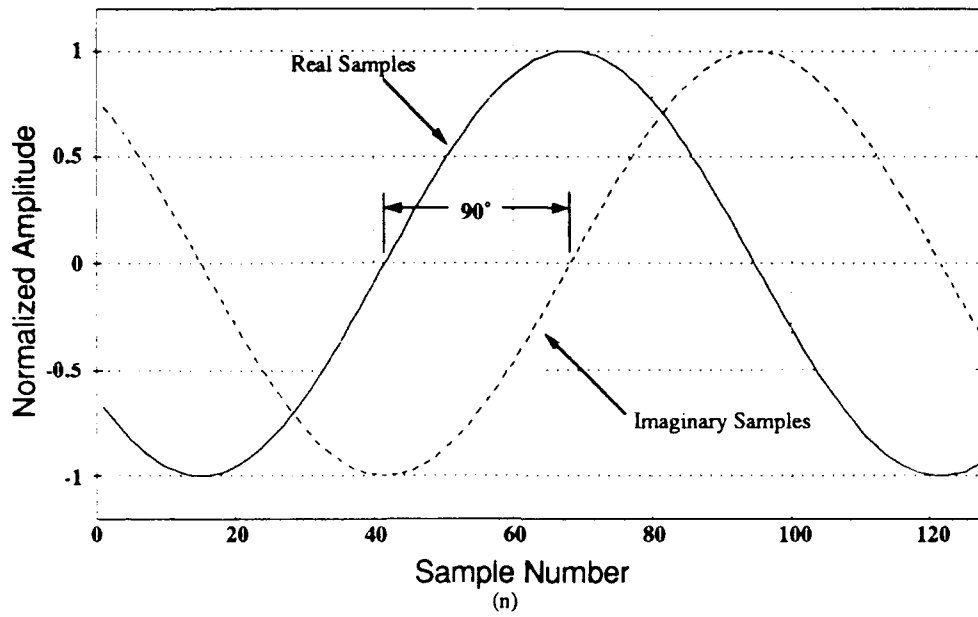


Figure B-5. Narrowband filter output spectrum, linear time epoch of sampled data.

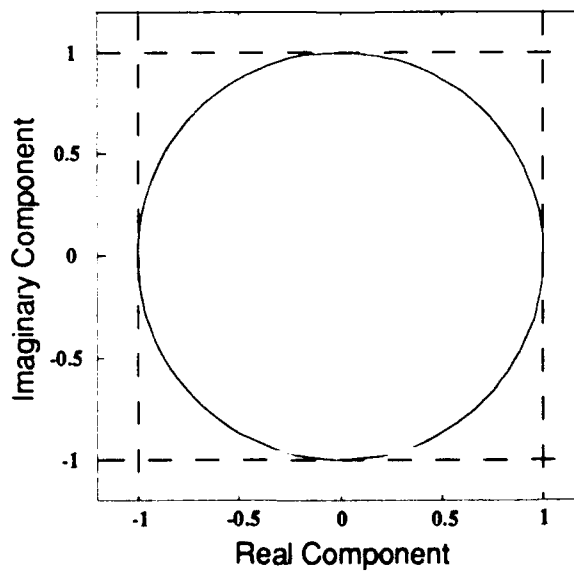


Figure B-6. Narrowband filter output spectrum, complex mapping of sample data.

